Magneto-optical transitions in multilayer semiconductor nanocrystals

2003 J. Phys.: Condens. Matter 15 3593

(http://iopscience.iop.org/0953-8984/15/21/308)

INSTITUTE OF PHYSICS PUBLISHING JOURNAL OF PHYSICS: CONDENSED MATTER

J. Phys.: Condens. Matter **15** (2003) 3593–3606 PII: S0953-8984(03)59304-3

Magneto-optical transitions in multilayer semiconductor nanocrystals

J Climente[1], J Planelles[1], W Jaskólski[2] and J I Aliaga[3]

[1] Departament de Ciències Experimentals, UJI, Box 224, E-12080 Castelló, Spain
[2] Instytut Fizyki UMK, Grudziądzka 5, 87-100 Toruń, Poland
[3] Departament d'Enginyeria i Ciència dels Computadors, UJI, Box 224, E-12080 Castelló, Spain

E-mail: planelle@exp.uji.es

Received 6 February 2003, in final form 31 March 2003
Published 19 May 2003
Online at stacks.iop.org/JPhysCM/15/3593

Abstract

Absorption spectra of chemically synthesized uniform and multilayer semiconductor nanocrystals in a magnetic field are investigated theoretically. The nanocrystals are modelled by spherical barrier/well potentials. The electron states are calculated within the effective mass model. A four-band $\boldsymbol{k}\cdot\boldsymbol{p}$ Hamiltonian, accounting for the valence subband mixing, is used to obtain the hole states. The magneto-optical transition spectrum depends strongly on the size and composition of the nanocrystals. In the case of small uniform quantum dots, only the linear Zeeman splitting of the electron and hole energy levels is observed even for very strong magnetic fields. In larger nanocrystals, the quadratic magnetic interaction turns out to be important and the transition spectrum becomes complicated. The most complicated influence of the magnetic field is found in quantum dot–quantum well systems in which the lowest electron and hole states are localized in a thin spherical layer. It is shown that transitions that are optically active when no magnetic field is applied remain strong even in very strong fields.

1. Introduction

The investigation of magnetic field effects in semiconductor quantum dots is of universal interest because the weaker quantum confinement and lighter electron effective mass than in atomic physics make it possible to observe effects that for natural atoms would require magnetic fields many orders of magnitude stronger than those accessible in the laboratory [1–6]. Such investigations are also of practical importance: magnetic fields can be used to tune quantum dot lasers and other optical nanodevices [7–10]. The application of external magnetic field to quantum dots, considered as qubits for quantum information processing [11], is thought of as a way to perform one-gate operations (spin rotations) and also to manipulate the tunnel barrier between coupled dots to perform multigate operations [12, 13].

Theoretical studies of magnetic field effects and magneto-optical transitions in quantum dots have dealt so far almost exclusively with two-dimensional disc-like or ring-like systems. In the majority of works, parabolic confining potentials and one-band models for both electrons and holes have been employed [1, 2]. The reason is twofold: both self-organized dots and rings proposed as quantum dot lasers and electrically gated dots proposed as qubits for quantum computing have rather planar geometry. On the other hand, two-dimensional models with parabolic potentials are particularly easy as regards numerical calculations.

Chemically synthesized nanocrystals have several advantages over other kinds of quantum dot. They are the smallest dots fabricated with the highest uniformity of sizes achieved in a given sample (only very recently has a size distribution as low as 2% for self-assembled PbSe quantum dots on PbTe quasisubstrates been reported [14]). They often have spherical shapes and are most similar to atoms. They can be synthesized as multilayer nanocrystals, i.e. built of concentric layers (shells) of different semiconducting materials with the shell thicknesses down to a single monolayer [9, 15, 16]. Electrons and holes can be localized in such structures within very thin spherical-like wells, which enhances the possibilities of tailoring their optical spectra. Two-dimensional and three-dimensional arrays of such nanocrystals reveal the highest density of nanoparticles and the strongest interactions between the neighbouring quantum dots [17, 18]. Such quantum dots are also considered as possible building blocks for future optoelectronic nanodevices and quantum computers.

In our previous works an extensive study of the magnetic field effects on the electron and hole energy levels of uniform and multilayer nanocrystals has been performed using a four-band $\boldsymbol{k}\cdot\boldsymbol{p}$ model that accounts for the valence subband mixing [19, 20]. To our knowledge, so far no detailed studies of e–h magneto-optical transition rates using this model have been made. In this paper we use the above-mentioned model to calculate e–h transitions for homogeneous and multilayer quantum dot–quantum barrier (QDQB) and quantum dot–quantum well (QDQW) nanocrystals, for a wide range of applied magnetic field.

2. Theory

In our model the conduction band states (electrons) are described by means of the one-band effective mass equation. For spherical nanostructures the electron wavefunction can be explicitly written as $\Psi_e = f_n^{lm}(r)|l, m\rangle|S\sigma\rangle$, where $f_n^{lm}(r)$ is the radial and $|l, m\rangle$ the angular part of the envelope function and $|S\sigma\rangle = |S\rangle|\sigma\rangle$ is the Bloch function, with $\sigma = \alpha$ or β. When an external magnetic field $\boldsymbol{B} = (0, 0, B)$ is applied, the spherical symmetry is lowered to axial symmetry and the electron wavefunction, written in cylindrical coordinates, is

$$\Psi_{F_z}^e = f_m^e(\rho, z)\mathrm{e}^{\mathrm{i}m\phi}|S\sigma\rangle. \tag{1}$$

The proper treatment of the valence band states (holes) requires taking into account the valence subband mixing. To this end we use the four-band $\boldsymbol{k}\cdot\boldsymbol{p}$ Hamiltonian, that couples the heavy-hole (HH) and light-hole (LH) subbands, and employ the envelope function approximation [21–24]. The use of the heavy-hole–light-hole (HH–LH) coupling opens new channels for dipole transitions in comparison to the single-band approximation. In the spherical case (no magnetic field present) the valence band states are eigenstates of the total angular momentum $\boldsymbol{F} = \boldsymbol{L}+\boldsymbol{J}$, where $\boldsymbol{J}$ is the Bloch angular momentum (the Bloch angular momentum quantum number for holes is $J = 3/2$) and $\boldsymbol{L}$ is the envelope angular momentum [25]. In axial symmetry, the Hamiltonian commutes only with the operator $\boldsymbol{F}_z$ of the projection of the total angular momentum $\boldsymbol{F}$ onto the field axis and the states are labelled only by F_z. To identify these states by their spherical notation at $B = 0$ we label them as (nQ_F, F_z), where Q denotes the spectroscopic notation for the lowest value of the envelope angular momentum L for a

given F [26]. The four-component hole function is [24]

$$\Psi^h_{F_z} = \sum_{M=F_z-3/2}^{F_z+3/2} f^h_M(\rho, z)\mathrm{e}^{\mathrm{i}M\phi}|3/2, J_z\rangle\delta_{J_z,(F_z-M)}, \tag{2}$$

where $|3/2, J_z\rangle$ are the Bloch functions for holes. The Hamiltonian eigenvalue problem reduces to the solution of coupled partial differential equations for the envelope function components $f^h_M(\rho, z)$ (or a single-differential equation for f^e_m). Finite-difference methods allow us to numerically solve these equations by transforming them into eigenvalue equations of huge, sparse, and asymmetric matrices. These matrices are diagonalized by the iterative Arnoldi solver [27] implemented in the ARPACK package [28].

Rates of optical transitions between the conduction and valence band states are calculated, excluding exciton effects[4]. The optical transition matrix element,

$$\begin{aligned}|\langle\Psi^e_{F'_z}|\boldsymbol{p}|\Psi^h_{F_z}\rangle|^2 &= \left|\sum_M \int f^e_m f^h_M \rho\,\mathrm{d}\rho\,\mathrm{d}z\,\delta_{mM}\langle S\sigma|\boldsymbol{p}|3/2, (F_z - M)\rangle\right|^2 \\ &= S^2_{eh}|\langle S\sigma|\boldsymbol{p}|3/2, (F_z - M)\rangle|^2\delta_{mM},\end{aligned} \tag{3}$$

is a product of the electron–hole overlap, S^2_{eh}, and the angular factor. The angular factor is calculated in terms of the square of the Kane parameter $P^2 = |\langle S|p_x|X\rangle|^2$ after explicitly writing the Bloch factors in terms of the eight band-edge basis functions $\{|S, 1/2\rangle, |S, -1/2\rangle, |X, 1/2\rangle, \ldots, |Z, -1/2\rangle\}$ [31].

Note that the symmetry selection δ_{mM}-rule selects, if any, only one of the four components of the hole function. Thus, for instance the transition between

$$\Psi^e = f^e_m|m = 1\rangle|S, \alpha\rangle \tag{4}$$

and

$$\Psi^h_{F_z=3/2} = \sum_{M=F_z-3/2}^{F_z+3/2} f^h_M(\rho, z)|M\rangle|3/2, (F_z - M)\rangle, \tag{5}$$

in z-polarized light, leaves only one term,

$$S^2_{eh}|\langle S\alpha|z|3/2, 1/2\rangle|^2 = S^2_{eh}\tfrac{2}{3}P^2, \tag{6}$$

of equation (3).

If we consider unpolarized light (i.e., we add all three (x-, y-, and z-) components of $\boldsymbol{p}$) and consider transition to both $|S\alpha\rangle$ and $|S\beta\rangle$, then the transition rate is just the overlap integral times the Kane parameter ($S^2_{eh}P^2$).

We perform the calculations for nanocrystals as large as 24 nm in diameter. The hole energy levels are closely spaced in such dots and a large number of hole states have to be taken into account to reliably model even the low-energy part of the magneto-optical transitions. In the case of the QDQB system, the total number of transitions that we calculate is 640 (128×5 field values). The hole wavefunctions, equation (2), have four components, each one being obtained on a two-dimensional (200×399) grid in a $\rho \times z$ array, thus being defined on 314 424 grid points. This requires parallel computation to get the solutions in a reasonable time. This is why we limit our calculations to the four-band approach. We have checked nonparabolicity effects on the conduction band in the case of small and large uniform quantum dots. The results obtained show a shift of the electron energy levels towards lower values and

[4] Although the e–h Coulomb interaction can yield some rearrangement of the energy levels, the main effect is a parallel shift of the entire spectrum toward lower energies [29]. In the case of the ground transition, this excitonic shift can be estimated using the Brus formula [30], that for the largest QD investigated yields ≈20 meV.

a moderate reduction of the splitting of the degenerate states produced by the magnetic field. However, these effects do not lead to essentially different results and conclusions and we have not considered nonparabolicity effects in the calculations.

3. Uniform nanocrystal

3.1. Small nanocrystals

In this section we study the evolution, versus magnetic field, of the low-energy electron–hole transition spectra for a small uniform (3 nm radius) InAs quantum dot. Such nanocrystals are routinely synthesized by wet chemistry methods and have almost spherical shapes with sizes in the range 2–10 nm [32]. In our study the surrounding medium is modelled by a 4 eV external potential barrier for both electrons and holes. The $\boldsymbol{k}\cdot\boldsymbol{p}$ parameters that we use are: effective electron mass $m^* = 0.024$; Luttinger parameters $\gamma_1 = 19.7$ and $\gamma = 8.4$ [34]. Although the magnetic field breaks the spherical symmetry, we use only two Luttinger parameters (spherical approximation) in order to make a proper comparison with the results obtained at zero magnetic field. The magnetic fields considered here range from $B = 0$ to 40 T in 10 T steps. Since the density of the hole energy levels is higher than the density of electron levels, we calculate transitions only between the 1s electron ground state and the five low-lying hole states, namely $1P_{3/2}$, $1S_{3/2}$, $1P_{5/2}$, $1D_{5/2}$, $2S_{3/2}$. This represents 24 doubly degenerate transitions to the electron states $1s|S\alpha\rangle$ and $1s|S\beta\rangle$.

When $B = 0$, the axial symmetry selection δ_{mM}-rule is supplemented by the spherical symmetry selection δ_{lL}-rule. Then, only the $1s \leftarrow 1S_{3/2}$ and $1s \leftarrow 2S_{3/2}$ transitions are allowed in the energy region studied (in spherical symmetry the hole wavefunctions have two components with angular momenta L and $L+2$).

When the magnetic field is on, the degenerate F_z-components of the $nS_{3/2}$ hole state split and the two transition bands ($n = 1, 2$), allowed at $B = 0$, also split into four components $(3/2, 1/2, -1/2, -3/2)$. Figure 1 shows the calculated e–h transitions versus magnetic field. For $B = 0$, only 8 transitions (out of the total number of 24 transitions calculated) are nonzero, yielding two sets of fourfold-degenerate $1s \leftarrow 1S_{3/2}$ and $1s \leftarrow 2S_{3/2}$ transitions. Since the nanocrystal studied is very small, the quantum confinement is strong, the energy levels are well separated, and one can easily follow the evolution of the spectrum with the magnetic field in figure 1. It is worthwhile emphasizing that transitions forbidden at $B = 0$ by the symmetry selection δ_{lL}-rule remain basically forbidden also for $B \neq 0$. For B as strong as 30 T, two additional very weak transitions (ten times weaker than the $1s \leftarrow 1(2)S_{3/2}$ ones) are seen at energies 2146 and 2048 meV. They correspond to $1s \leftarrow 1D_{5/2}$ ($F_z = \pm 1.5$). At $B \sim 30$ T the $1D_{5/2}$ ($F = 1.5$) state anticrosses with $1P_{5/2}$ ($F = 1.5$) and for $B = 40$ T a slightly stronger $1s \leftarrow 1P_{5/2}$ ($F_z = 1.5$) transition is seen in between the $\pm F_z$-components of the $1s \leftarrow 2S_{3/2}$ transition.

Note that when $B \neq 0$, just 20 out of the 24 calculated transitions corresponding to $1P_{3/2}$, $1S_{3/2}$, $1P_{5/2}$, $1D_{5/2}$, $2S_{3/2}$ hole states are allowed by the symmetry selection δ_{mM}-rule, but even at $B = 40$ T, only 8 of them (those fulfilling the δ_{lL}-rule) are strong. This is because in small nanocrystals the radius of the maximum charge density is much smaller than the radius of the lowest Landau orbit, $\left[2|F_z + 1|\frac{\hbar}{eB}\right]^{1/2}$, for the fields considered. Thus, only the linear Zeeman, and not the quadratic term, is important (see figure 1) and the quantum dot states are negligibly influenced by the field.

3.2. Large nanocrystals

Let us consider now a larger homogeneous InAs nanocrystal of radius 8 nm. The weaker confinement yields a higher density of electron and hole energy levels, which now start to cross

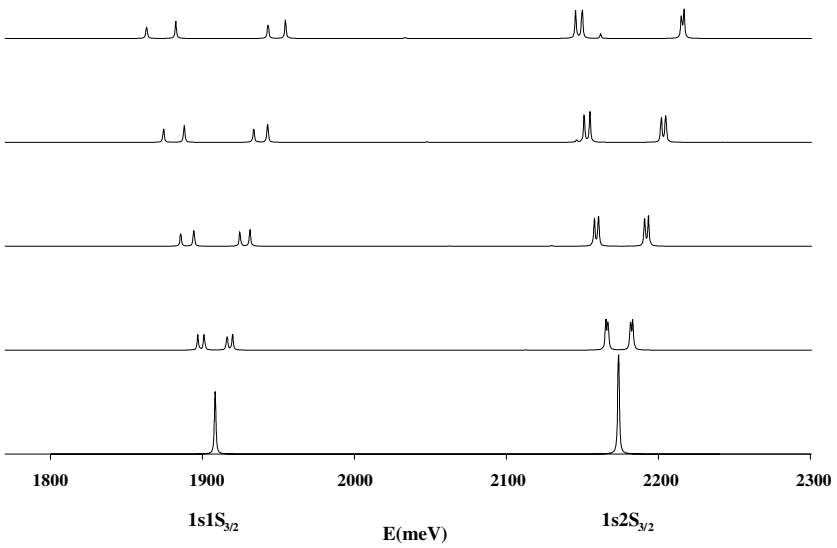

Figure 1. The low-energy part of the magneto-optical spectrum of the spherical uniform InAs nanocrystal of radius 3 nm. The spectra at different fields, from $B = 0$ (bottom) up to $B = 40$ T (top) in 10 T steps, are offset. Transitions at $B = 0$ are explicitly labelled. Transition positions are given in millielectronvolts, while the absorption intensity is given in arbitrary units. The spectrum is modelled by adding 1 meV wide Lorentzian envelopes to the transition strengths.

and mix for weaker fields. Thus, we include in the calculations of the transition rates not only the 1s ground electron state but also the first excited state, 1p (components $1p_{-1}$, $1p_0$, $1p_{+1}$), and the $m = -2$ component of the second excited 1d state. We consider 12 hole states in the transitions to the 1s electron ground state and 5 hole states in transitions to the excited 1p and $1d_{-2}$ electron states. Thus, we take into account 74 transitions to the 1s electron state (they come from $1S_{3/2}$, $1P_{3/2}$, $1P_{5/2}$, $1D_{5/2}$, $2S_{3/2}$, $2P_{3/2}$, $1D_{7/2}$, $1F_{7/2}$, $1F_{9/2}$, $3S_{3/2}$, $1G_{9/2}$, and $2D_{5/2}$ hole states). However, the symmetry selection δ_{mM}-rule reduces this number to 48 transitions (twelve low-lying hole states of the four allowed $F_z = 3/2, 1/2, -1/2, -3/2$ components). Adding the number of the possible transitions to the 1p and $1d_{-2}$ electron state, we end up with the total number of 128 transitions calculated.

Figure 2 shows the evolution of the low-energy spectrum of the e–h transitions for five values of the magnetic field (0, 10, 20, 30, and 40 T). At $B = 0$, only five transitions are seen; from left to right they are: $1s \leftarrow 1S_{3/2}$, $1s \leftarrow 2S_{3/2}$, $1s \leftarrow 3S_{3/2}$, $1p \leftarrow 1P_{3/2}$, and $1p \leftarrow 1P_{5/2}$. When the magnetic field is on, both the electron and hole levels split into $2k + 1$ components ($k = l$ for the electrons and F for holes). Thus, the $1s \leftarrow nS_{3/2}$ transition splits into four components, while $1p \leftarrow 1P_{3/2}$ splits into ten components (not 12, because $1p_1(m = +1) \leftarrow 1P_{3/2}$ ($F_z = -3/2$) and $1p_1$ ($m = -1$) $\leftarrow 1P_{3/2}$ ($Fz = 3/2$) are forbidden by the symmetry selection δ_{mM}-rule). Finally, $1p \leftarrow 1P_{5/2}$ splits into 12 components (not 18, for similar reasons). At $B = 10$ T the components of $1s \leftarrow nS_{3/2}$, $n = 1, 2, 3$, are well separated. This is not the case for the $1p \leftarrow 1P_{3/2}$ and $1p \leftarrow 1P_{5/2}$ transitions, whose components appear mixed in the energy region considered.

Looking at figure 2 we can see that, at $B = 10$ T, there are six transitions in the region between 720 and 750 meV (in fact there are seven transitions located at 721, 725, 727, 732, 742, 743, and 744 meV, but the ones arising at 742 and 743 overlap, so only one wider transition is seen). Only four of them can arise from the $1s \leftarrow 2S_{3/2}$ transition. They

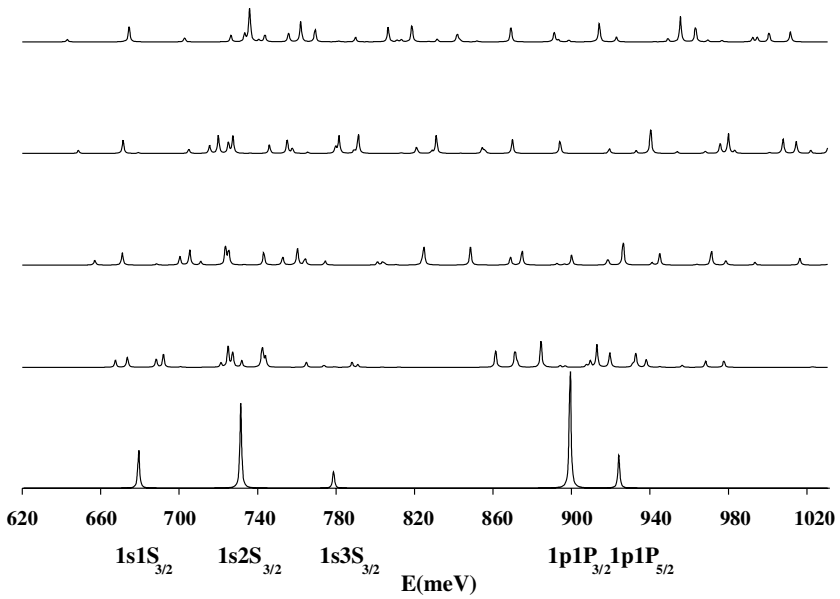

Figure 2. As figure 1, but for a large InAs nanocrystal of radius 8 nm.

appear at 721, 725, 742, and 743 meV for the F_z-components equal to -1.5, -0.5, 0.5, 1.5 of $1s \leftarrow 2S_{3/2}$, respectively. The first one is weak and the others are strong. The additional three optically active transitions in this region are: $1s \leftarrow 1D_{7/2}$ ($F = -1.5$) at 727 meV, $1s \leftarrow 1D_{5/2}$ ($F = 1.5$) at 732 meV and $1s \leftarrow 2P_{3/2}$ ($F = 0.5$) at 744 meV. The latter two transitions are weak but the $1s \leftarrow 1D_{7/2}$ ($F = -1.5$) is strong. This is due to a strong interaction between the $2S_{3/2}$ ($F_z = -1.5$) and $1D_{7/2}$ ($F_z = -1.5$) hole states that anticross at $B = 10$ T and to a large extent 'exchange' their wavefunctions.

For B between 20 and 40 T, more transitions appear to be optically active in the energy range investigated. The hole states $1D_{5/2}$ ($F = 1.5$) and $2P_{3/2}$ ($F = 0.5$) undergo anticrossings with $1P_{5/2}$ ($F = 1.5$) and $1D_{7/2}$ ($F = 0.5$) and the transitions from these states to 1s become stronger. Simultaneously, the components $F_z = 1.5$ and 0.5 of the transition $1s \leftarrow 2S_{3/2}$ become weaker.

In summary, the most remarkable feature of the evolution of the transition spectrum versus magnetic field is that, except for a few weak transitions, the transitions that are strong for $B \neq 0$ correspond basically to the ones that split from the transitions allowed at $B = 0$. In some cases, when the hole levels of the same symmetry (the same F_z) anticross, the labelling of the corresponding transitions can change, as happens at $B = 10$ T for the $1s \leftarrow 2S_{3/2}$ and $1s \leftarrow 1D_{7/2}$ ($F = -1.5$) transitions discussed above. Another remarkable anticrossing and 'exchange' of the hole wavefunctions occurs for $1S_{3/2}$ ($F_z = -1.5$) and $1P_{3/2}$ ($F_z = -1.5$), which for $B > 10$ T becomes the lowest transition. The strength of this transition decreases as the field increases and its energy distance to the next optically active transition increases simultaneously (see figure 2). This effect should be seen in an experiment as a dark or weak magnetoexciton.

Since tracing the evolution of the different components in the transition spectrum shown in figure 2 is difficult, we present in figure 3 the same spectrum but for z-polarized light and including only transitions to the $|S\alpha\rangle$ electron component. Under these conditions only transitions from the hole ($F_z - 1/2$) component are allowed, so the $1s \leftarrow nS_{3/2}$, $n = 1, 2, 3$,

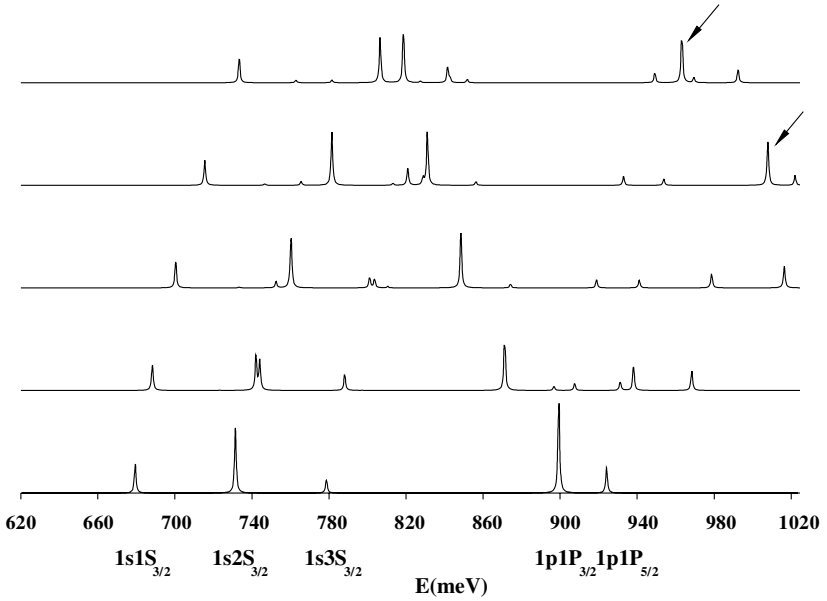

Figure 3. The low-energy part of the magneto-optical spectrum of a spherical uniform InAs nanocrystal of radius 8 nm for z-polarized light and including only transitions to the $|S\alpha\rangle$ electron components.

do not split and the $1s \leftarrow 1P_{3/2}$, $1s \leftarrow 1P_{5/2}$ split into three components (p_0, p_{+1}, and p_{-1}). The resulting spectrum is simple enough for one to see how it evolves with the field and that the transitions forbidden at $B = 0$ continue to be very weak for the increasing field. Two strong transitions indicated by arrows in figure 3 correspond to $1d_{-2} \leftarrow 1D_{5/2}$ ($F_z = -2.5$), a high-energy transition allowed at $B = 0$, that significantly lowers in energy when the field increases.

4. Quantum dot–quantum barrier systems

In this section we consider a three-layer nanocrystal built of an internal InAs core of radius 7 nm, a middle InP shell of thickness 1 nm, and an external 3.5 nm InAs cladding. Since the forbidden energy gap of InAs is narrower than the gap of InP, the middle shell acts as a barrier separating two spherical InAs wells (barrier height [33]: 0.52 eV for electrons and 0.42 eV for holes). As before, the surrounding medium is modelled by a 4 eV external potential barrier. Since we are mainly interested in the states having energies below the InP barrier and thus expect a small charge density in the barrier region, the effective mass and Luttinger parameters of InAs are used for the whole nanocrystal.

As in the case of a large homogeneous nanocrystal, the weak confinement leads also here to a dense distribution of the energy levels. Then, excited transitions enter into the low-energy region of the spectrum as the magnetic field increases. In this case we have included in the calculations the 1s, 1p (+1, 0, −1), and 1d (−2, −1) electron states and eight low-lying hole states for the four allowed F_z-components. Thus, since the δ_{mM}-rule yields $M = m = 0$ for all transitions to the ground electron state 1s ($m = 0$), the allowed F_z-values are: 1.5, 0.5, −0.5, and −1.5 (see equation (2)), and the eight low-lying hole states included in the calculations are: $1P_{3/2}$, $1S_{3/2}$, $1P_{5/2}$, $2S_{3/2}$, $1D_{5/2}$, $2P_{3/2}$, $3S_{3/2}$, and $1D_{7/2}$. In a similar way, we calculate

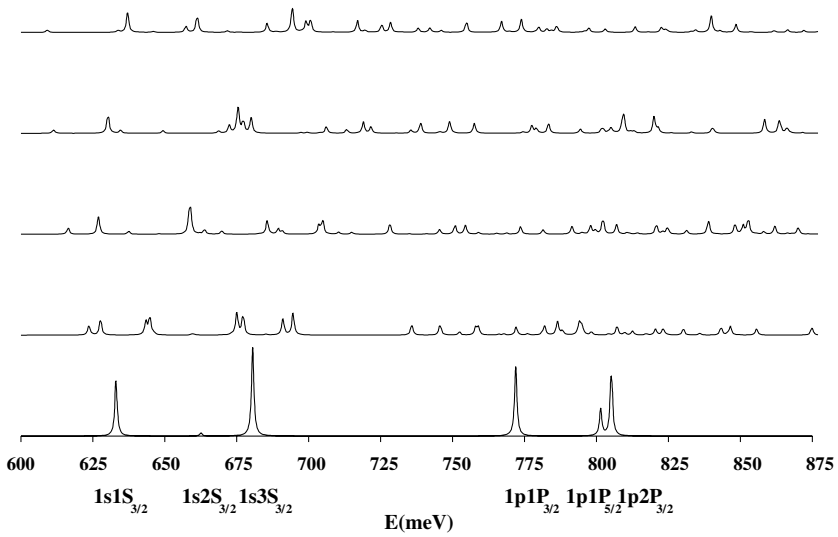

Figure 4. The low-energy part of the magneto-optical spectrum of a spherical multishell InAs (7 nm)/InP (1 nm)/InAs (3.5 nm) QDQB nanocrystal. The spectra at different fields, from $B = 0$ (bottom) up to $B = 40$ T (top) in 10 T steps, are offset. Transitions at $B = 0$ are explicitly labelled. The transition positions are given in millielectronvolts, while the absorption intensity is in arbitrary units. The spectrum is modelled by adding 1 meV wide Lorentzian envelopes to the transition strengths.

all allowed transitions to the excited electron states. For example, all the hole states involved in transitions to the $1p_{-1}$ electron state are the $F_z = 0.5$, -0.5, and -1.5 components of the above hole states and, additionally, the $F_z = -2.5$ component of $1P_{5/2}$, $1D_{5/2}$, $1D_{7/2}$, $2P_{5/2}$, $2D_{5/2}$, $1F_{7/2}$, $1F_{9/2}$, and $2F_{7/2}$ states. Altogether, there are 320 transitions, but only 184 are allowed in axial symmetry and must be calculated for each value of the magnetic field.

Figure 4 summarizes the evolution of the low-energy part of the e–h transition spectrum of the QDQB system versus the magnetic field. At $B = 0$ only six allowed transitions are seen. They are: $1s \leftarrow 1S_{3/2}$, $1s \leftarrow 2S_{3/2}$, $1s \leftarrow 3S_{3/2}$, $1p \leftarrow 1P_{3/2}$, $1p \leftarrow 1P_{5/2}$, and $1p \leftarrow 2P_{3/2}$.

At first glance the magnetic field dependence of the QDQB transition spectrum goes along similar lines to that for the homogeneous nanocrystal (figure 2): the $1s \leftarrow nS_{3/2}$ transitions are well separated at low magnetic field and the $1p \leftarrow nP_{k/2}$ ones are mixed, even for very small B-values. However, there are several differences caused by the presence of a thin InP barrier in the QDQB system. First, the $1p \leftarrow 2P_{3/2}$ transition appears very close to the $1p \leftarrow 1P_{5/2}$ one. This is because the $2P_{3/2}$ hole state builds its charge density mainly in the external InAs cladding with a node in the region of the InP barrier, while the charge density of the $1P_{5/2}$ state is mostly localized in the internal well, which allows for similar energies of the corresponding energy levels [19]. The second and most striking difference is a reversal of the relative intensities of the $1s \leftarrow 2S_{3/2}$ and $1s \leftarrow 3S_{3/2}$ transitions. Again, it can be explained by the presence of the InP barrier in the QDQB structure: the intensities are proportional to the overlap integral for the electron envelope function and one of the components of the hole envelope. Figure 5 shows the $L = 0$ component of the $1S_{3/2}$, $2S_{3/2}$, and $3S_{3/2}$ states for both the homogeneous nanocrystal and the QDQB system. The corresponding electron envelope functions are also shown. One can see how the barrier influences the shape of the hole wavefunction, being responsible for the weak $1s \leftarrow 2S_{3/2}$ and strong $1s \leftarrow 3S_{3/2}$ transitions in the QDQB system. It is also worthwhile to note that although in this case the lowest transition,

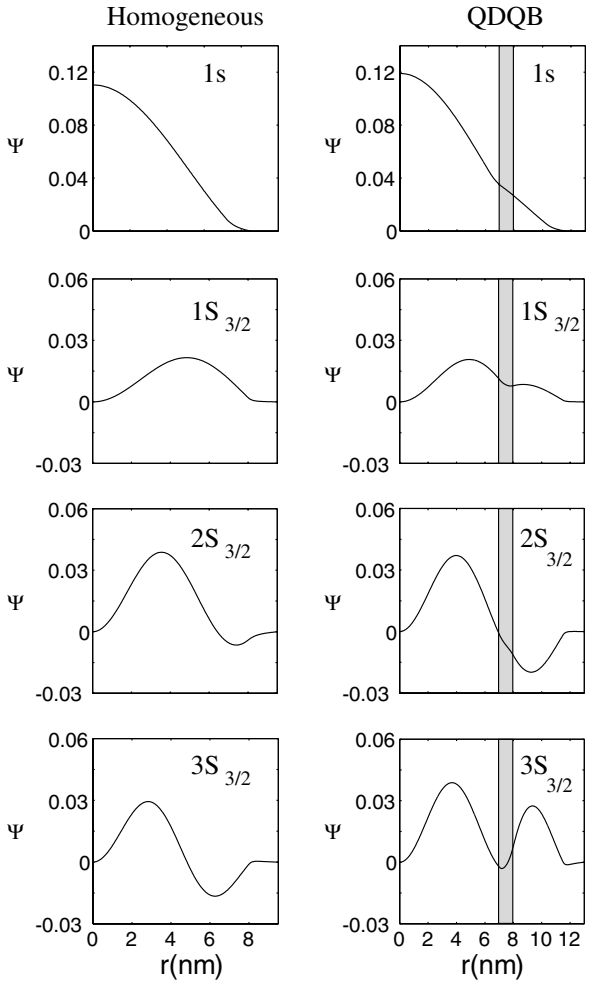

Figure 5. The envelope component with $L = 0$ of the hole states $1S_{3/2}$, $2S_{3/2}$, $3S_{3/2}$ of both the spherical uniform InAs nanocrystal of radius 8 nm and the spherical multishell InAs (7 nm)/InP (1 nm)/InAs (3.5 nm) QDQB nanocrystal. The corresponding 1s electron envelope functions are also shown.

$1s \leftarrow 1S_{3/2}$ ($F_z = -1.5$), does not cross with the $1p \leftarrow 1P_{3/2}$ transition, its intensity decreases when the magnetic field increases.

Some of the hole states, which at $B = 0$ build significant parts of their charge densities in the external cladding, may undergo crossovers to the internal core in the strong magnetic field [19]. Since this usually does not happen for the corresponding electron state in a given transition, such a transition progressively lowers in intensity, as happens, for example, to the $1p \leftarrow 2P_{3/2}$ transition. Another difference, also caused by a density crossover, is the ordering of the split components of the $1s \leftarrow 3S_{3/2}$ transition. In homogeneous nanocrystals the ordering (versus increasing energy) is $F_z = -3/2, -1/2, 1/2, 3/2$ (as it is for every $F = 3/2$ splitting in the homogeneous nanocrystal). This is not the case in the QDQB system. At $B = 10$ T the sequence of the levels in the QDQB structure is $F_z = -3/2, -1/2, 3/2, 1/2$. This reordering can be understood by looking at the hole wavefunctions. At $B = 0$ T the $3S_{3/2}$ ($F_z = 3/2$) state has the maximum of its charge density localized in the external

cladding, while this is not the case for the $3S_{3/2}$ ($F_z = 1/2$) state. When $B < 10$ T the energy of the $3S_{3/2}$ ($F_z = 3/2$) state almost does not increase, since its charge density in the external cladding does not change much (it only slightly concentrates in two regions close to the z-axis). For $B > 10$ T a crossover occurs and the $3S_{3/2}$ ($F_z = 3/2$) state starts to increase in energy faster than the $3S_{3/2}$ ($F_z = 1/2$) state (as is the rule for uniform dots).

5. Quantum dot–quantum well systems

Let us consider now a three-layer nanocrystal built of an internal barrier-acting InP core, a middle well-acting InAs shell, and an external barrier-acting InP cladding. The radius of the core is 8 nm, the thickness of the InAs shell is 2 nm, and the external InP cladding is 2 nm thick. The band offset is 0.52 eV for electrons and 0.42 eV for holes [33], and the height of the surrounding barrier is assumed to be 4 eV (from the bottom of the InAs well). Since we are investigating the bound states having charge densities localized mainly in the middle shell, the electron effective mass and valence band Luttinger parameters of InAs are, for simplicity, used for the whole structure.

In the QDQW system investigated, the density of the electron and holes states is even higher than in the structures studied in the previous sections. Additionally, the effect of a periodic change of the electron ground state energy versus magnetic field induces changes in the low-energy part of the spectrum as the field strength increases. Therefore, in order to study the evolution of the low-energy part of the e–h transition spectrum, we include the 1s, 1p ($m = 1, 0, -1$), and 1d ($m = -2, -1$) electron states. For each electron state we consider transitions from the five low-lying hole states for all the allowed F_z-components. The total number of transitions that we deal with is 236, but the symmetry selection δ_{mM}-rule reduces the number of calculations to 120 transitions for each value of the magnetic field.

In order to give insight into the complication of the transition spectrum, we plot in figure 6 the transition energies of all the transitions studied, disregarding the fact that many of them may have negligible intensity. This can be seen in figure 7, where all transition energies are represented by vertical bars, while the spectrum is modelled by adding 1 meV wide Lorentzian envelopes to the transition strengths. Figure 6 helps us to see how the transition energies cross as the magnetic field increases and, in particular, how the energies of the excited transitions decrease. The numerous crossings observed and the progressive change of the symmetry of the lowest transition are direct consequences of the behaviour of the electron and hole energy levels of QDQW structures in a magnetic field, reported by us in [19, 20].

As seen in figure 7, the transitions $1s \leftarrow nS_{3/2}$, for $n > 1$, do not appear in the low-energy region. This is because the second state of each symmetry is pushed towards higher energies, since it must have a node in the well (just the opposite to what happens in the QDQB system). When the field is on, the multiplets split and even at $B = 10$ T the spectrum becomes complicated. At $B = 30$ T the transition that is the lowest one at $B = 0$, i.e. $1s \leftarrow 1S_{3/2}$ ($F_z = -1.5$), is exceeded by two other transitions: weak $1p_1 \leftarrow 1P_{5/2}$ ($F_z = -2.5$) and strong $1p_1 \leftarrow 1P_{3/2}$ ($F_z = -1.5$) transitions, and overlaps with two strong transitions, namely $1d_{-2} \leftarrow 1D_{5/2}$ ($F_z = -2.5$) and $1p_1 \leftarrow 1P_{3/2}$ ($F_z = -0.5$). It is worth pointing out an important difference between the QDQW system and all the other nanocrystals studied: while for the uniform and the QDQB nanocrystals the low-energy part of the transition spectrum reflects the behaviour of the hole energy levels in a magnetic field, the structure of the QDQW transition spectrum is governed mainly by the evolution of the electron ground state symmetry versus B.

Since tracing the evolution of the different components in the QDQW transition spectra shown in figure 7 is extremely difficult, we present in figure 8 the same spectrum but for

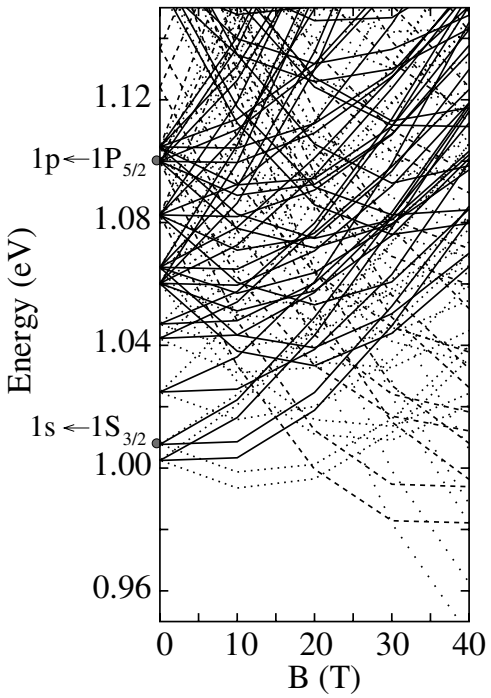

Figure 6. Transition energies (meV) versus magnetic field (T) for a spherical multilayer InP (8 nm)/InAs (2 nm)/InP (3 nm) QDQW nanocrystal. Full curves: $|F_z| = 0.5$; dashed curves: $|F_z| = 1.5$; densely dotted curves: $|F_z| = 2.5$; and dotted curves: $F_z = -3.5$. Allowed transitions at $B = 0$ are explicitly labelled.

z-polarized light and including only transitions to the electron $|S\alpha\rangle$ components. Under these conditions only transitions from the hole ($F_z - 1/2$) component are allowed, so the $1s \leftarrow 1S_{3/2}$ state does not split and both $1p \leftarrow 1P_{3/2}$ and $1p \leftarrow 1P_{5/2}$ split into three components (p_0, p_{+1}, and p_{-1}). The quadratic effect is so pronounced in the QDQW structure that even in this very simplified spectrum it is difficult to trace the evolution of the transitions. In order to help the reader, the lines connecting the same states for different fields are included. This figure confirms again that the strong signals observed at high fields are basically the ones that split from the transitions allowed at $B = 0$.

6. Concluding remarks

We have investigated magneto-optical transitions in uniform InAs and multilayer InAs/InP nanocrystals by using a one-band model for the electron states and a four-band $\boldsymbol{k} \cdot \boldsymbol{p}$ approach to describe the hole states. We have shown that in the case of small uniform quantum dots, the linear Zeeman splitting of the electron and hole energy levels alone determines the structure of the transition spectrum in magnetic fields up to 40 T, leading to linear and symmetric splitting of the transition components of similar strengths. In a large uniform nanocrystal the quadratic magnetic effects also becomes important. With increasing magnetic field the strong splitting of the energy levels, degenerate at $B = 0$, yields a mixing of the components belonging to different transitions and the magnetoabsorption spectrum becomes complicated. It has been found that in high magnetic fields the lowest energy component ($F_z = -1.5$) of the ground state

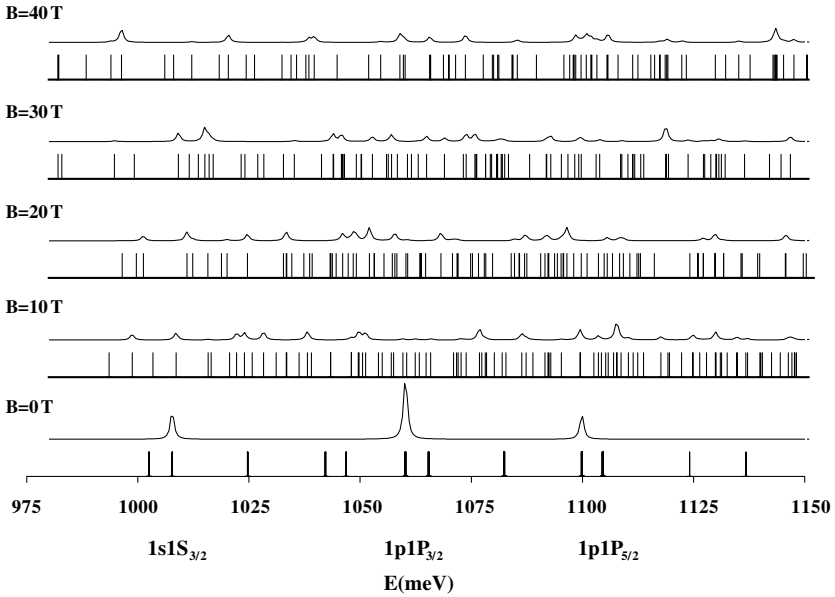

Figure 7. As figure 4, but for a spherical multishell InP (8 nm)/InAs (2 nm)/InP (3 nm) QDQW nanocrystal.

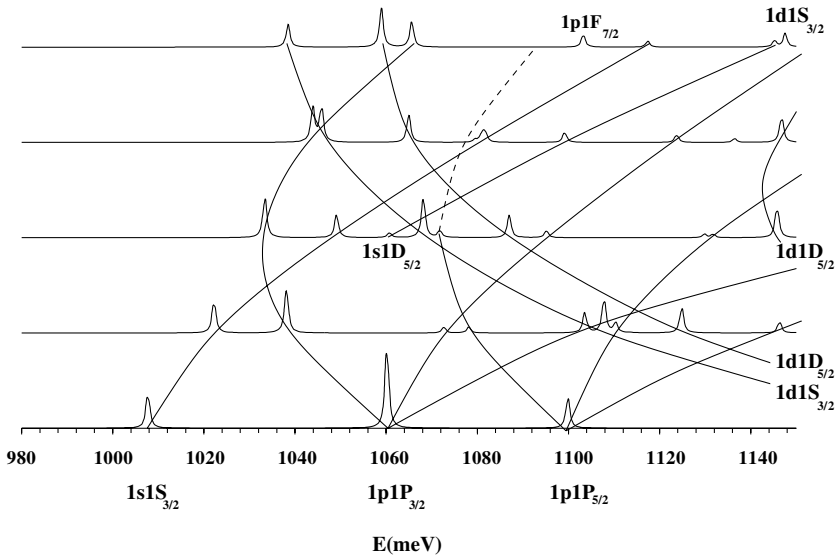

Figure 8. The low-energy part of the magneto-optical spectrum of a spherical multishell InP (8 nm)/InAs (2 nm)/InP (3 nm) QDQW nanocrystal with z-polarized light and including only transitions to the $|S\alpha\rangle$ electron components. The spectrum is modelled by adding 1 meV wide Lorentzian envelopes to the transition strengths.

transition ($1s \leftarrow 1S_{3/2}$) becomes very weak and increases its distance to the next optically active transition, which should be seen in experiment as a dark magnetoexciton. We have shown that magneto-optical spectra of chemically synthesized multilayer nanocrystals differ

significantly for nanocrystals of different size, composition, and sequence of layers. Many differences observed between the spectra of uniform and QDQB structures have been explained as results of the presence of a thin InP barrier-acting shell in multishell nanocrystals. We have shown that the transition spectrum depends strongly on whether the thin middle shell is a well-acting or barrier-acting layer. This can be important in the modelling of such nanocrystals as potential building blocks for optoelectronic nanodevices. It has also been found that transitions that are allowed at $B = 0$ are also allowed for higher fields, although their labelling can change due to anticrossings of the energy levels.

Acknowledgments

Financial support from Generalitat Valenciana CTIDIB-2002/189, UJI-Bancaixa P1-B2002-01 and KBN-8T11B06218 is gratefully acknowledged. The MCT-FPU (JC) FPU grant is also acknowledged.

References

[1] Jacak L, Hawrylak P and Wójs A 1998 *Quantum Dots* (Berlin: Springer)
[2] Chakraborty T 1999 *Quantum Dots* (Amsterdam: Elsevier)
[3] Bylicki M and Jaskólski W 1999 *Phys. Rev.* B **60** 15924
[4] Jaskólski W, Bosek M, Bylicki M and Planelles J 2001 *Vacuum* **63** 185
[5] Lorke A, Luyken R J, Govorov A O, Kotthaus J P, Garcia J M and Petroff P M 2000 *Phys. Rev. Lett.* **84** 2223
[6] Lieb E H, Solovej J P and Yngvason J 1995 *Phys. Rev.* B **51** 10646
[7] Bimberg D, Grundmann M and Ledentsov N N 2001 *Quantum Dot Heterostructures* (Chichester: Wiley)
[8] Sadowski M L, Potemski M and Gyuberg M 1999 *Optical Properties of Semiconductor Nanostructures (NATO ASI Series vol 81)* (Dordrecht: Kluwer)
[9] Woggon U 1997 *Optical Properties of Semiconductor Quantum Dots* (Berlin: Springer)
[10] Ando T, Arakawa Y, Foruka K, Komiyama S and Nakashima H (ed) 1998 *Mesoscopic Physics and Electronics* (Berlin: Springer)
[11] Awschalom D D, Los D and Samarth N (ed) 2002 *Semiconductor Spintronics and Quantum Computation* (Berlin: Springer)
[12] Loos D and DiVincenzo D P 1998 *Phys. Rev.* A **57** 120
[13] Burkard G and Loss D 2002 *Europhys. News* **33** 166
[14] Alchalabi K, Zimin D, Kostorz G and Zogg H 2003 *Phys. Rev. Lett.* **90** 026104-1
[15] Mews A, Eychmüller A, Giersig M, Shoos D and Weller H 1994 *J. Phys. Chem.* **98** 934
Mews A, Kadavanich A V, Banin U and Alivisatos A P 1996 *Phys. Rev.* B **53** R13242
[16] Little R B, El-Sayed M A, Bryant G W and Burke S 2001 *J. Chem. Phys.* **114** 1813
[17] Jaskólski W, Bryant G W, Planelles J and Zieliński M 2002 *Int. J. Quantum Chem.* **90** 1075
[18] Döliefeld H, Weller H and Eychmüller A 2001 *Nano Lett.* **1** 267
Artemyev M V, Bibik A I, Gurinovich L I, Gaponenko S V and Woggon U 1999 *Phys. Rev.* B **60** 1504
Kagan C R, Murray C B, Nirmal M and Bawendi M G 1996 *Phys. Rev. Lett.* **76** 1517
[19] Planelles J, Climente J, Díaz J G and Jaskólski W 2002 *J. Phys.: Condens. Matter* **14** 1
[20] Planelles J, Díaz J G, Climente J and Jaskólski W 2002 *Phys. Rev.* B **65** 245302
[21] Bányai L and Koch S W 1993 *Semiconductor Quantum Dots* (Singapore: World Scientific)
[22] Baldereschi A and Lipari N O 1973 *Phys. Rev.* B **42** 2697
Gregorian G B, Kazaryan E M, Efros Al L and Yazeva T V 1990 *Sov. Phys.–Solid State* **32** 1031
[23] Xia J B 1989 *Phys. Rev.* B **40** 8500
[24] Planelles J, Jaskólski W and Aliaga I 2001 *Phys. Rev.* B **65** 033306
[25] Sercel P C and Vahala K J 1990 *Phys. Rev.* B **42** 3690
[26] Efros Al L and Rosen M 1998 *Phys. Rev.* B **58** 7120
[27] Arnoldi W E 1951 *Q. J. Appl. Math.* **9** 17
Saad Y 1992 *Numerical Methods for Large Scale Eigenvalue Problems* (New York: Halsted)
Morgan R B 1996 *Math. Comput.* **65** 1213

[28] Lehoucq R B, Sorensen D C, Vu P A and Yang C 1998 ARPACK: Fortran subroutines for solving large scale eigenvalue problems (release 2.1)
Lehoucq R B, Sorensen D C and Yang C 1998 *ARPACK User's Guide: Solution of Large-Scale Eigenvalue Problems with Implicit Restarted Arnoldi Methods* (Philadelphia, PA: SIAM)
[29] Raymond S, Fafard S, Poole P J, Wójs A, Hawrylak P, Charbonneau S, Leonard D, Leon R, Petroff P M and Merz J L 1996 *Phys. Rev.* B **54** 11548
Raymond S, Hawrylak P, Gould P, Fafard S, Sachradja A, Potemski M, Wójs A, Charbonneau S, Leonard D, Petroff P M and Merz J L 1997 *Solid State Commun.* **101** 883
[30] Brus L E 1984 *J. Chem. Phys.* **80** 4403
[31] Bastard G 1988 *Wave Mechanics Applied to Semiconductor Heterostructures* (Les Ulis: Les Éditions de Physique)
[32] Banin U, Lee C J, Guzelian A A, Kadavanich A V, Alivisatos A P, Jaskólski W, Bryant G W, Efros Al L and Rosen M 1998 *J. Chem. Phys.* **109** 2306
[33] Cao Y W and Banin U 2000 *J. Am. Chem. Soc.* **122** 9692
[34] Madelung O (ed) 1982 *Numerical Data and Functional Relationships in Science and Technology, group III, vol 17 Landolt–Börnstein New Series* (Berlin: Springer)